AVO analysis on CRS gathers - a 3D land data example from Mexico

Blas de la Peña*, Lucas Freitas, Nikita Shuliko, Rodolfo Ballesteros (Geoprocesados)
Jorge Barrios, Camilo Viniegra, Julio Perez Aldana, Tomas Perez, Arturo Ramirez (PEMEX)

Abstract

A case study for a 3D land data from Mexico illustrates the contribution of CRS processing to AVO analysis. The CRS supergather shows itself as a powerful tool in AVO analysis, decreasing drastically the crossplot dispersion. Its trade-off are a slight smoothing on the amplitude variations and on spatial resolution.

Introduction

Amplitude variation with offset (AVO) analysis has been proven to be an effective tool for hydrocarbon detection. The offset variations in seismic reflection amplitude provide an estimative of elastic and lithological parameters like porosity, lithology and fluid content. Anomalous behavior of such variations can be used to detect certain areas, e.g., gas-sand areas are usually indicated by an increase in absolute amplitude with the offset (Ostrander, 1984).

The processing flow for AVO analysis is meant to be amplitude preserving, in the sense that try to make the input data compatible to the Shuey's equation (Cambois 2001). The most common factors that interferes such compatibility are amplitude corrections, wavelet variations, residual NMO, residual multiple energy and noise. (Graul, 2001). The latter's effect in AVO attributes has been proven to be very harmful (Koza, 2003; Hatchel, 2000; Simm, 2000).

In this case study, we compare the results of AVO analysis over output of three different processing flows: (i) non amplitude preserving, (ii) amplitude preserving (Resnick, 1993) and (iii) amplitude preserving together with CRS technique (Baykulov, 2008).

Geological setting and exploration objectives

The onshore study area is located in the Salina del Istmo Basin in Mexico, south of the Gulf of Mexico and in the northern part of the Istmo of Tehuantepec (Figure 1). This basin covers parts of the states of Veracruz and of Chiapas, in southern Mexico. Several producing oil fields are located in this area, such as Sanchez Magallanes, Blasillo, San Ramon, and Cinco Presidentes. Lithologically, these oil fields are associated with Miocene sands. Their structures are dominated by strong salt tectonics. In this area there is a close relationship between the presence of amplitude anomalies and hydrocarbons.

Figure 1: Study area

For this case study, a 3D reflection seismic dataset is selected from an onshore survey that was acquired in the 1990s in the Salina del Istmo Basin. The referred area contains a producing field, as illustrated in Figure 2.

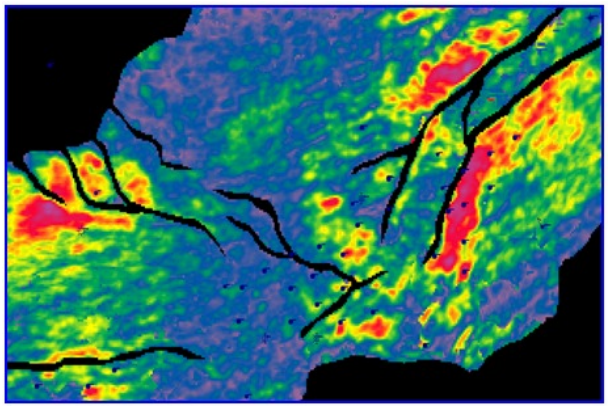

Figure 2: RMS amplitude along a top horizon indicating the reservoir location

An initial AVO analysis performed using the available processed dataset not only identified class III anomalies at the reservoir but also in an extense area at variables depths. Such false anomalies were generated by a prior "AVO unfriendly" processing sequence that resulted in a downscale of amplitudes for near offsets (see Figure 3).

In this context, the client asked us to reprocess this dataset using an appropriate sequence. The design of such flow was based on well established sequences (Resnick, 1993:

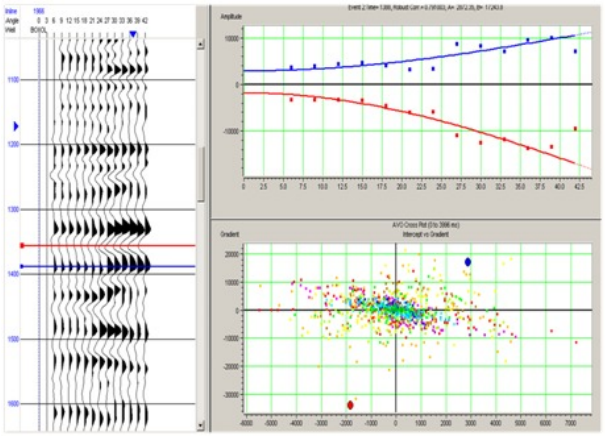

Figure 3: Gather with amplitude problems and its erroneous classification as a class III anomaly

Feng, 2006) and considered the crucial issues elucidated by Combois (Combois, 2001).

The CRS method

In the time processing, the CRS or Common-Reflection-Surface method was applied in order to compensate for the imaging problems in the low-fold areas as well as increase dataset's signal-to-noise ratio. The processing steps that preceded the CRS are the ones from a standard time workflow until the final application of residual statics and, therefore, are not in the scope of this work. For more information on these topics, the reader should refer to (Ylmaz,2001).

The CRS stack (Tygel,1997; Mller,1999) is a technique which aims to obtain optimum simulated zero-offset volumes by stacking the multicoverage dataset along multi-parameter surfaces determined in a data-driven way. The stacking operator is of second order in the half-offset and midpoint coordinates. Thus, for each zero-offset sample to be simulated, stacking is performed not only along a trajectory restricted to the one CMP gather but along an entire surface in time-midpoint-offset space, locally approximating the corresponding traveltime surface in the prestack data over several CMPs. The much higher stacking fold results in a significantly improved S/N ratio.

CRS stacking operators depend on a number of parameterscalled CRS attributes, kinematic wavefield attributes or wavefront attributeswhich determine their shapes. In the 3D case, the three CRS attributes are denoted by two 2x2 symmetric matrices M_ξ and M_h and 1x2 vector p which are the traveltime derivatives. The CRS operator for a zero-offset sample (ξ_0, t_0) as a function of midpoint displacement ξ and half-offset h then reads

$$t^2(\xi,h) = (t_0 + 2p\xi)^2 + \xi^T M_\xi \xi + h^T M_h h$$

Therefore, associated to the simulated zero-offset volume there are a number of attribute volumes (three volumes in 2D and eight in 3D). These volumes consist in the optimum attribute values determined by means of coherence analysis.

As described by Muller (2003), these traveltime derivatives contain information about the normal ray and the so called eigenwaves (Hubral, 1983). These are two hypothetical waves that start at the normal-incident point (NIP) and propagate upwards with half the medium velocity: the NIP wave propagates from a point source; while the N wave propagates from an exploding reflection element.

The first order derivative estimated for a zero-offset sample (ξ_0, t_0) relates to the emergence angles of the normal ray which emerges at ξ_0 , and has two-way traveltime t_0 The second order derivatives, on the other hand, give information about the curvature of the associated eigenwaves (K_N and K_{NIP}) observed at ξ_0. More specifically,

$$\begin{aligned} p &= \frac{1}{2}\frac{\partial t}{\partial \xi} = \frac{1}{v_0}[sin(\alpha)cos(\phi), sin(\alpha)sin(\phi)]^T \\ M_\xi &= \frac{1}{2}\frac{\partial^2 t}{\partial \xi^2} = \frac{1}{v_0} H K_N H^T \\ M_h &= \frac{1}{2}\frac{\partial^2 t}{\partial h^2} = \frac{1}{v_0} H K_{NIP} H^T \end{aligned}$$

where v_0 is the near surface velocity, and H is the transformation matrix from measured surface coordinates to local ray-centered Cartesian coordinates determined by two subsequent rotations in azimuth ϕ and dip α direction.

CRS Gather

As mentioned above, the CRS methodology is based on a second order approximation of the reflection event on both half-offset and midpoint coordinates. A schematic description of both iso-offset curves of traveltime, in blue, and the CRS approximation, in green is presented in Figure 4.

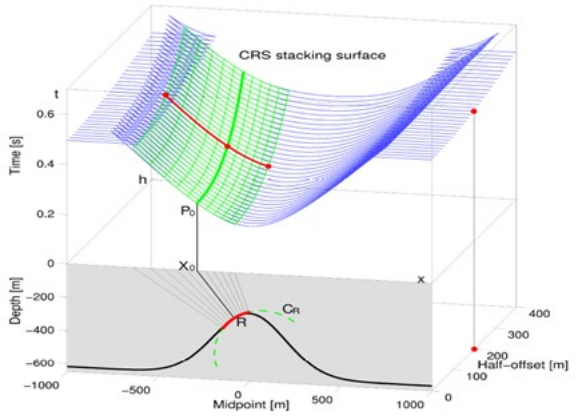

Figure 4: The CRS operator (green) and the partial stacking (red) for a given offset

The CRS gather is generated by partial stacking along the midpoint direction, i.e., along the red lines in Figure 8 (Baykulov, 2008). In practice, it is determined in two steps: First, a moveout-corrected gather is extracted from the dataset by direct application of the CRS attributes and stacking only in the midpoint direction. Then conventional moveout recovery and regularization is applied. As expected, the generated gathers present an excellent signal-to-noise ratio when compared to the input CMP gathers (see Figure 6).

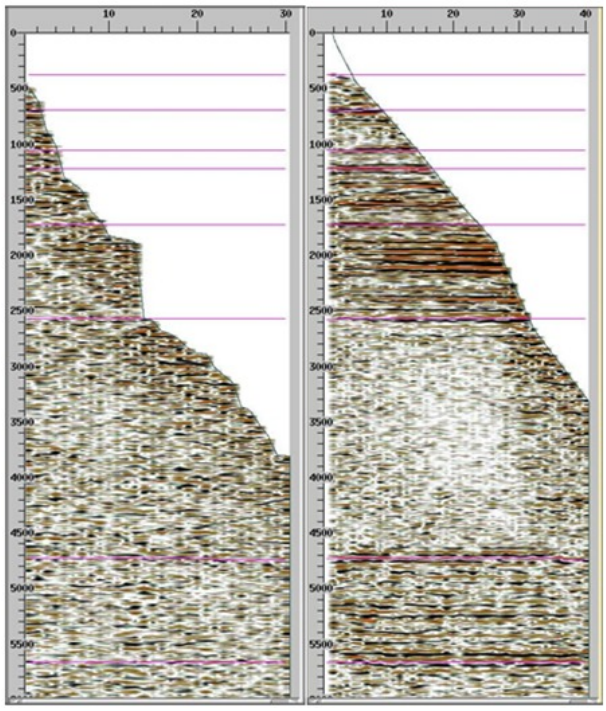

Figure 5: Input CMP gather (left) and the corresponding CRS gather (right)

The enhance in signal-to-noise in the CRS gathers are reflected not only at the PSTM volumes (Figure 6) but also at the AVO crossplots we will show in the next sections.

AVO analysis

Zoeppritz equations describes how the energy of a plane wave is partitioned into reflected, reflected and converted, transmitted and converted waves, after inciding at a plane interface (Aki, 1980). According to these equations, the reflection coefficient variation with the incident angle is dependent on changes in medium P-wave velocity (Vp), S-wave velocity (Vs) and density (rho). Anomalously low ratios caused by hydrocarbons produce anomalous variation with offset. These amplitude analysis became more practical after approximations (Shuey, 1985; Aki 1980). One of the most used is Shuey's two term equation. In this approximation, the reflection coefficient of the P-wave is given by

$$R(\theta) \quad = \quad A + B sin^2(\theta)$$

where θ is the incidence angle, A is the normal incidence reflection coefficient or "intercept", and B is the AVO slope or "gradient". These coefficients derivate other AVO attributes like fluid factor and gas indicator.

AVO crossplotting facilitates the interpretation of the AVO response. Each response is represented as a single point on a crossplot of intercept and gradient. The points related to brine-saturated sandstones and shales follow a well-defined "background" trend. Anomalous responses are properly viewed as deviations from this background and may be related to hydrocarbons or lithological factors. This graphical tool allows an easy classification of AVO response into four categories, see Figure 8. Moreover, the use of crossplots are recommended to avoid inappropriate results (Castagna, 1997).

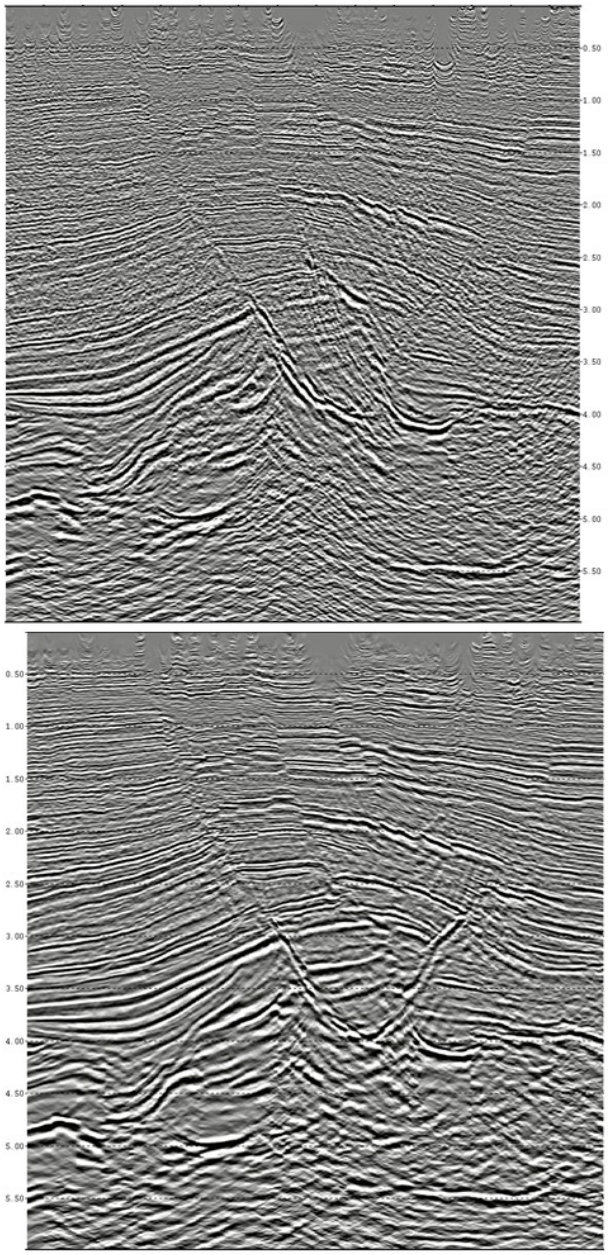

Figure 6: Inline of migrated volumes using conventional processing (top) and using CRS technique (bottom)

Results and Discussion

Amplitude preservation in the reprocessing flow is a key factor in order to perform AVO analysis. The obtained results were confirmed by comparing the results of AVO analysis with available information from several well calibrations.

Figure 8 presents the AVO curves and crossplots using AVO Attributes Intercept and gradient for the same location of Figure 3 for both processing flows, with and without CRS. There is no evidence of an AVO anomaly, as we expected, so we can conclude that both workflows were performed

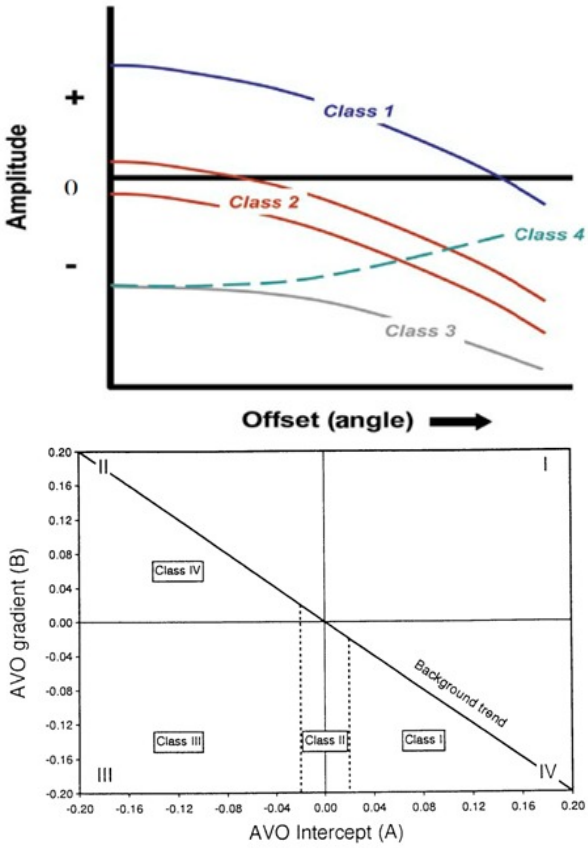

Figure 7: Amplitude behavior with offset (top) and crossplot location (bottom) of each class.

AVO friendly.

An oil producing well interval is shown in Figure 9. The clear evidence of a class III AVO anomaly is present in both process, but the greater dispersion in the crossplot of the flow without CRS is related to the higher amount of random noise (Cambois, 2000). However, the responses of the CRS-based flow show a slight smooth in the amplitude curves. It can also be seen that the distance of the anomaly from the background is greater in the CRS-based flow than in the conventional, what simplifies the identification of AVO anomalies in the whole volume.

Figure 10 presents a comparison for a oil producing interval in another well. As before, both crossplots show a class III AVO anomaly clearly. However, the anomaly points (red and blue points) of the CRS-based flow present larger deviation from the background trend (and also distance from each other). The higher signal-to-noise ratio of CRS-based processing flow is reflected as a smaller point dispersion. Such feature provide a improvement in data continuity and in AVO anomaly definitions.

The same enhances are observed when performing AVO analysis for a region rather than for a single location. Figure 11 shows crossplots of a region for both processing workflows. The fluid factor of each point is showed in colorscale. High values of fluid factor (red and blue) are related to hydrocarbon presence, while low values (yellow) indicate water saturation. As one can see, the

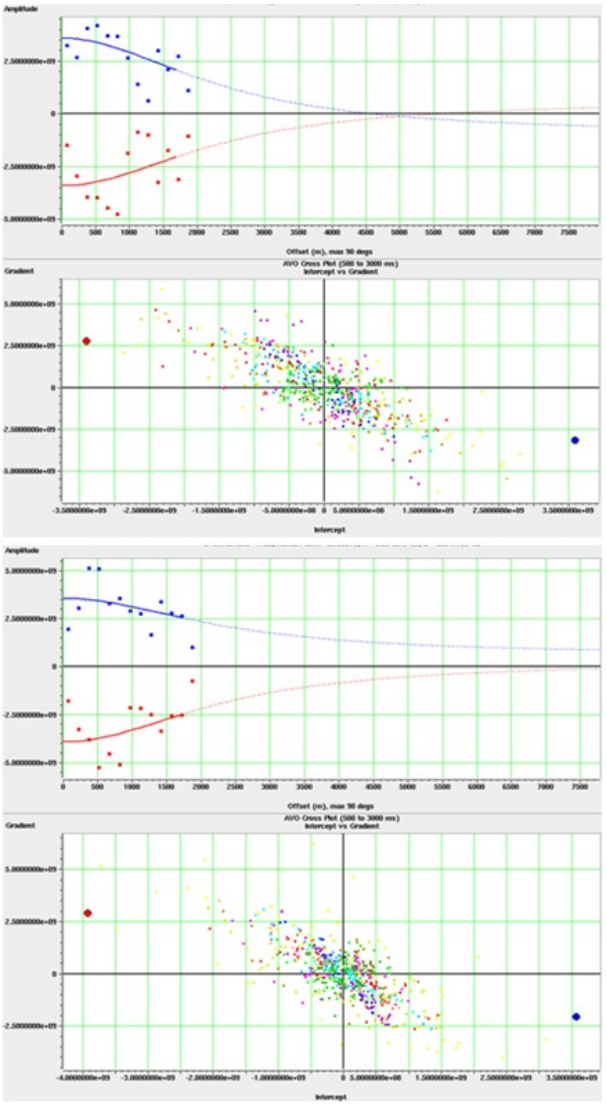

Figure 8: AVO responses of same location of Figure 3, after the AVO friendly reprocessing, with (bottom) and without CRS (top).

class III anomalies deviation from the background is much higher for the CRS-based processing flow. This drastically simplifies the identification of such anomalies.

Figure 12 shows the class III AVO anomalies identified in all over the seismic volume by the selection presented in Figure 11. Note that the well log (red and blue solid lines) shows a very good correlation between oil saturated sand and the presented anomalies.

As the result of the AVO analysis, we proposed several well locations for the client. One of them is the directional well depicted in Figure 12 (black solid line). It is clear how the AVO anomaly stops against a fault zone (red dashed line), what makes te latter a good oil trap.

Conclusions

This case study shows that the CRS technique may be incorporated into AVO friendly processing workflow improving the results of a subsequent AVO analysis. As

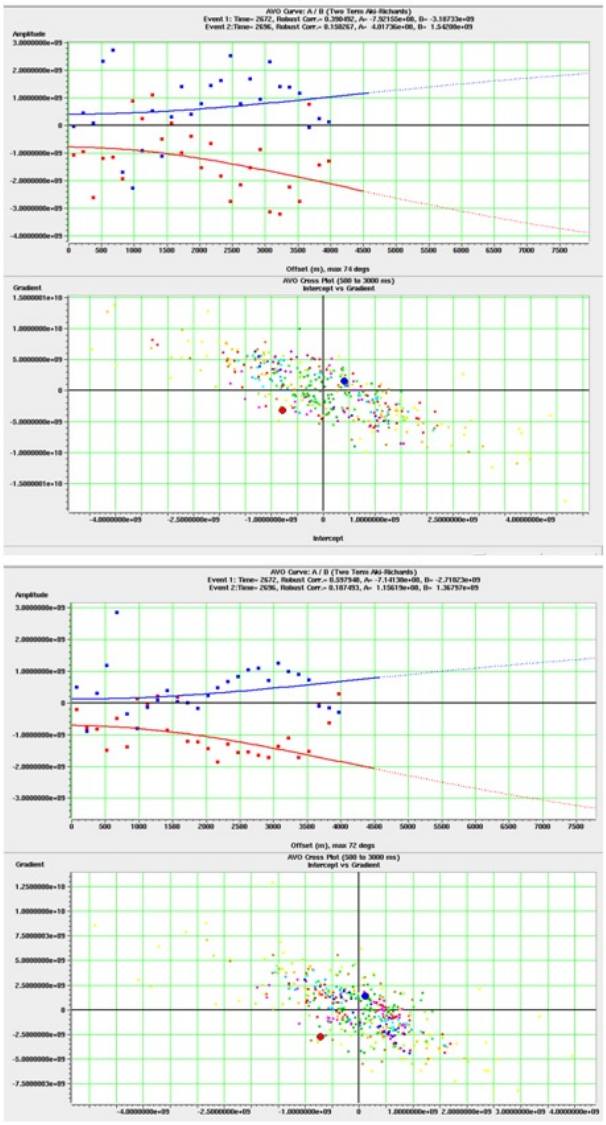

Figure 9: Crossplots for the reprecessing with (bottom) and without CRS (top). Note the greater dispersion on the top crossplot.

illustrated by several examples, the generation of CRS gathers do not compromise the amplitude behavior of AVO curves. Conversely the use of CRS gathers leads to enhanced AVO anomalies by reducing dispersion and increasing the anomaly deviations from the background.

Acknowledgements

We thank PEMEX for the permission to present their data.

References

Aki, K., Richards, P.G., 1980. Quantitative seismology: Theory and methods. W.H. Freeman and Co.

Baykulov, M. and Gajewski, D., 2008. Prestack seismic data enhancement with CRS parameters, *70th EAGE Conference Exhibition, Ext. Abstr.*

Cambois, G., 2000. Can P-Wave AVO be Quantitative?. em The Leading Edge, 19, 1246-1251.

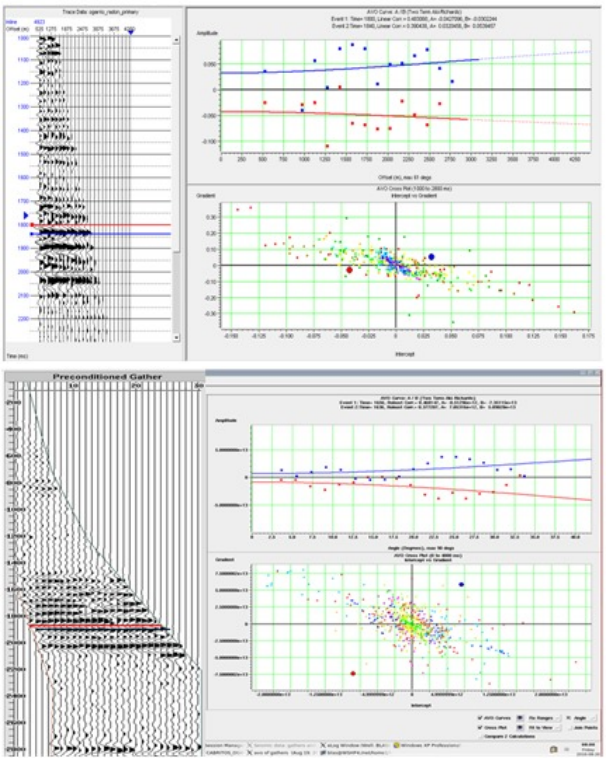

Figure 10: Crossplots at another oil producing interval for the reprecessing with (bottom) and without CRS (top).

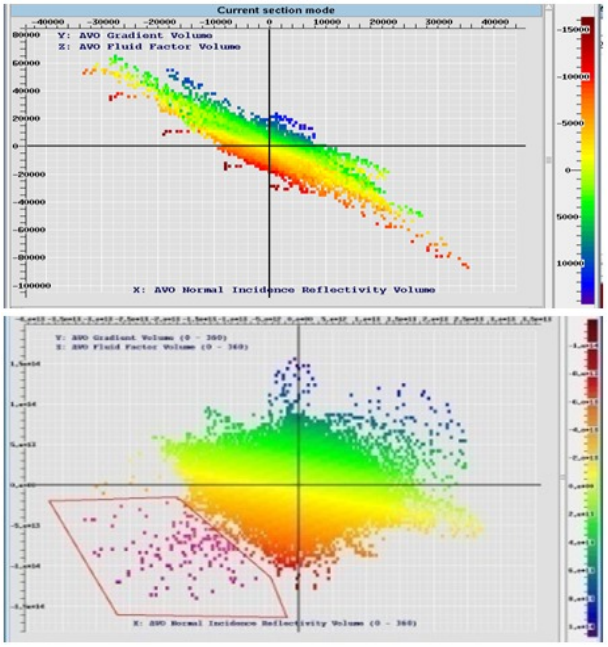

Figure 11: Crossplots for a region of the the reprecessed datasets. At the top, conventional processing flow and at the bottom, flow with CRS.

Cambois, G., 2001. AVO Processing: Myths and Reality. em CSEG Recorder,2001

Castagna, J.P., Swan, H.W., 1997. Principles of AVO

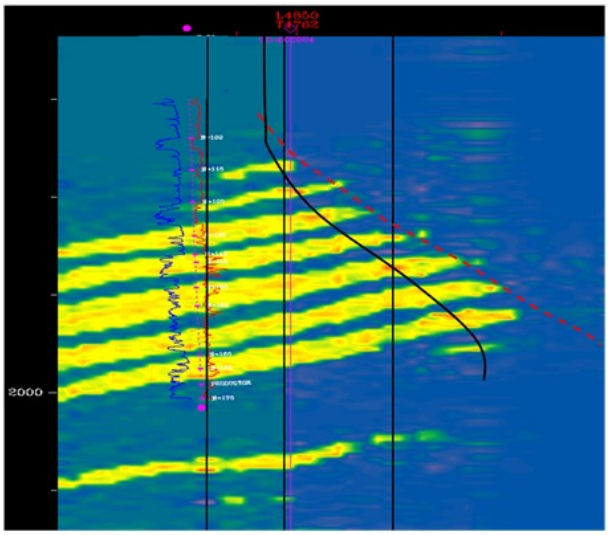

Figure 12: Fluid factor attribute for the class III locations selected in Figure 11 together with interpreted fault (red dashed), a proposed well location (back solid), and well logs (blue and red solid).

crossplotting. *The Leading Edge*, 16, 337-344

Feng, H., Bancroft, J.C., 2006. AVO principles, processing and inversion. *CREWES Research Report*, 18.

Graul, M. 2001. AVO: Yesterday, today and (a peek at) tomorrow. *CSEG Recorder*, 2001

Hatchell, P. J., 2000. Fault whispers: Transmission distortions on prestack seismic reflection data.*Gephysics*, 65, 377-389

Hubral, P., 1983. Computing true amplitude reflections in laterally inhomogeneous earth. *Geophysics*, 48, 1051-1062

Koza, S., Castagna, J.P., 2003. The effects of noise on AVO crossplots. *SEG Expanded Abstracts*, 22, 274-277

Müller, A. 2003. The 3D Common-Reflection-Surface: Theory and Application, PhD thesis, Karlsruhe University.

Müller, T. 1999. The common reflection surface stack method: PhD thesis, Karlsruhe University

Ostrander, W., 1984. Plane-wave reflection coefficients for gas sands at nonnormal angles of incidence. *Gephysics*, 49, 1637

Resnick, J. R. 1993. Seismic data processing for AVO and AVA analysis. *In Offset Dependent Reflectivity - Theory and Practice of AVO Analysis*, Society of Exploration Geophysicists, Tulsa Oklahoma.

Shuey, R.T., 1985. A simplification of Zoeppritz equations.*Geophysics*, 50, 609-614

Simm, R., White, R., Uden, R., 2000. The anatomy of AVO crossplots.*The Leading Edge*, 19, 150-155

Tygel, M. T. Muller, P. Hubral, J. Schleicher, 1997. Eigenwave based multiparameter traveltime expansions. *SEG Expanded Abstracts* 16, 1770

Yilmaz, O., 2001. Seismic Data Analysis: Processing, Inversion and Interpretation of Seismic Data. Society of Exploration Geophysicists, Tulsa Oklahoma.